Non-specific activities of the major herbicide-resistance gene BAR

Christ, Bastien ; Hochstrasser, Ramon ; Guyer, Luzia ; Francisco, Rita ; Aubry, Sylvain ; Hörtensteiner, Stefan ; Weng, Jing-Ke

Abstract: Bialaphos resistance (BAR) and phosphinothricin acetyltransferase (PAT) genes, which convey resistance to the broad-spectrum herbicide phosphinothricin (also known as glufosinate) via N-acetylation, have been globally used in basic plant research and genetically engineered crops 1-4 . Although early in vitro enzyme assays showed that recombinant BAR and PAT exhibit substrate preference toward phosphinothricin over the 20 proteinogenic amino acids 1 , indirect effects of BAR-containing transgenes in planta, including modified amino acid levels, have been seen but without the identification of their direct causes 5,6 . Combining metabolomics, plant genetics and biochemical approaches, we show that transgenic BAR indeed converts two plant endogenous amino acids, aminoadipate and tryptophan, to their respective N-acetylated products in several plant species. We report the crystal structures of BAR, and further delineate structural basis for its substrate selectivity and catalytic mechanism. Through structure-guided protein engineering, we generated several BAR variants that display significantly reduced non-specific activities compared with its wild-type counterpart in vivo. The transgenic expression of enzymes can result in unintended off-target metabolism arising from enzyme promiscuity. Understanding such phenomena at the mechanistic level can facilitate the design of maximally insulated systems featuring heterologously expressed enzymes.

DOI: https://doi.org/10.1038/s41477-017-0061-1

Nonspecific activities of the major herbicide-resistance gene BAR

Authors: Bastien Christ[1], Ramon Hochstrasser[2]†, Luzia Guyer[2], Rita Francisco[2], Sylvain Aubry[2], Stefan Hörtensteiner[2]* and Jing-Ke Weng[1,3]*

[1] Whitehead Institute for Biomedical Research, 455 Main Street, Cambridge, MA 02142-1479, USA.

[2] Department of Plant and Microbial Biology, University of Zurich, Zollikerstrasse 107, CH-8008 Zurich, Switzerland.

[3] Department of Biology, Massachusetts Institute of Technology, Cambridge, MA 02139, USA.

*Correspondence to. Email: shorten@botinst.uzh.ch (S.H.); wengj@wi.mit.edu (J.K.W.)

† Present address: Institute of Medical Microbiology, University of Zurich, Gloriastrasse 30/32, CH-8006, Zurich, Switzerland

Bialaphos resistance (BAR) and phosphinothricin acetyltransferase (PAT) genes, which convey resistance to the broad-spectrum herbicide phosphinothricin (also known as glufosinate) via N-acetylation, have been globally used in basic plant research and genetically engineered crops[1-4]. Although early in vitro enzyme assays showed that recombinant BAR and PAT exhibit substrate preference toward phosphinothricin over the 20 proteinogenic amino acids[1], indirect effects of BAR-containing transgenes *in planta*, including modified amino acid levels, have been seen but without the identification of their direct causes[5,6]. Combining metabolomics, plant genetics, and biochemical approaches, we show that transgenic BAR indeed converts two plant endogenous amino acids, aminoadipate and tryptophan, to their respective N-acetylated products in several plant species examined. We report the crystal structures of BAR, and further delineate structural basis for its substrate selectivity and catalytic mechanism. Through structure-guided protein engineering, we generated several BAR variants that display significantly reduced nonspecific activities compared to its wild-type counterpart *in vivo*. Our results demonstrate that transgenic expression of enzymes can result in unintended off-target metabolism arising from enzyme promiscuity. Understanding of such phenomena at the mechanistic level can facilitate the design of maximally insulated systems featuring heterologously expressed enzymes.

Phosphinothricin is a naturally occurring herbicide derived from the tripeptide antibiotic bialaphos produced by species of *Streptomyces* soil bacteria. Phosphinothricin is a structural analog of glutamate, and thereby inhibits glutamine synthetase, an essential enzyme for glutamine synthesis and ammonia detoxification in plants, giving rise to its

herbicidal activity[3]. In the 1980s, the bialaphos resistance (*BAR*) gene and its closely related homolog phosphinothricin acetyltransferase (*PAT*) gene were isolated from *Streptomyces hygroscopicus* and *Streptomyces viridochromogenes*, respectively, and were later broadly used as transgenes to confer herbicide resistance in a variety of major genetically-engineered (GE) crops, including corn, soybean, canola, and cotton[7]. In addition, *BAR* and *PAT* have also gained much utility in basic research as selection markers for generating transgenic plants[1]. Despite the prevalent use of *BAR* and *PAT* in the context of generating herbicide-resistant transgenic plants, whether these bacteria-derived enzymes may possibly interfere with plant endogenous metabolism has not been rigorously investigated.

In research not initially intended to address this issue regarding phosphinothricin-resistance trait, we carried out untargeted metabolomics analysis on senescent leaf extracts prepared from the *Arabidopsis thaliana clh2-1* mutant (FLAG_76H05, referred to as FLAG-1 hereafter), which contains a transfer DNA (T-DNA) insertion that abolishes the *CHLOROPHYLLASE 2* gene[8]. This analysis revealed two metabolites that were ectopically accumulated at high levels in *clh2-1* compared to wild type (Fig. 1a). Using liquid chromatography-tandem mass spectrometry (LC-MS^2), we identified these two metabolites as N-acetyl-aminoadipate and N-acetyl-tryptophan (referred to as acetyl-aminoadipate and acetyl-tryptophan, respectively, hereafter; Fig. 1a and Supplementary Fig. 1). Because the deficiency of CHLOROPHYLLASE 2, a serine esterase[8], in *clh2-1* does not explain the accumulation of these acetylated metabolites, we hypothesized that the *BAR* gene present on the T-DNA as a selection marker in *clh2-1* might be responsible for their formation. To test this, we extended our metabolomics analysis to additional

Arabidopsis T-DNA insertional mutants unrelated to chlorophyll metabolism that carry either *BAR* (e.g. mutants from the FLAG[9] and SAIL[10] collections) or alternative antibiotic selection markers (e.g. mutants from the SALK (*NTPII*, kanamycin resistance)[11] and GABI (*SULI*, sulfadiazine resistance)[12] collections (Supplementary Table 1). Senescent leaves of all six T-DNA mutants carrying *BAR* manifested accumulation of acetyl-aminoadipate and acetyl-tryptophan, while these metabolites were significantly lower or not detected in wild-type plants and T-DNA mutants containing alternative selection markers (Fig. 1b). These results indicate that the ectopic accumulation of these metabolites is likely resulted from the nonspecific N-acetyltransferase activities of transgenic BAR acting upon plant endogenous amino acids.

We quantified the absolute concentrations of acetyl-aminoadipate and acetyl-tryptophan in senescent leaves of *BAR*-containing transgenic Arabidopsis to range from 306 to 845 nmole/g and from 14 to 76 nmole/g fresh weight, respectively (Supplementary Fig. 2). While trace level of acetyl-tryptophan can be detected in wild-type Arabidopsis, acetyl-aminoadipate was undetectable in wild-type samples (Supplementary Fig. 2). The ectopic accumulation of acetyl-aminoadipate and acetyl-tryptophan in *BAR*-containing transgenic Arabidopsis is substantial given that the concentrations of free aminoadipate and tryptophan in senescent leaves of these Arabidopsis lines are in the ranges of 61 to 122 nmole/g and from 1566 to 2663 nmole/g fresh weight, respectively (Supplementary Fig. 2). On the other hand, the concentrations of free amino acids in senescent leaves do not seem to be significantly affected by the expression of BAR, as revealed by the quantification of 21 other amino acids (Supplementary Fig. 2).

To assess whether the nonspecific activities of transgenic BAR also manifest in other plant hosts, we performed metabolic profiling of various tissue samples from phosphinothricin-resistant soybean (*Glycine max*), canola (*Brassica napus*), mustard (*Brassica juncea*) and wheat (*Triticum aestivum*). Substantially increased accumulation of acetyl-aminoadipate and acetyl-tryptophan was also detected in some tissues of these transgenic lines (Supplementary Fig. 3), indicating that our findings regarding the *in vivo* nonspecific activities of BAR may apply broadly to a wide range of *BAR*-containing transgenic plants.

The concentration of free tryptophan is low in photosynthetically active leaves, but increases significantly in senescent leaves[13]. This is due to enhanced proteolysis during senescence, facilitating remobilization of protein-bound nitrogen and other nutrients to sink organs, such as seeds[14]. Aminoadipate, an intermediate of lysine degradation, also exhibits a similar accumulation pattern during leaf senescence[15]. To test whether the BAR-catalyzed production of acetyl-aminoadipate depends on lysine degradation, we analyzed an Arabidopsis mutant from the FLAG collection, FLAG_*lkrsdh*, in which the *BAR*-containing T-DNA disrupts *At4g33150* encoding the Arabidopsis bifunctional lysine-ketoglutarate reductase/saccharopine dehydrogenase (LKR/SDH, Supplementary Fig. 4)[16]. LKR/SDH catalyzes the first committed step of lysine degradation, and, together with the subsequent aminoadipate semialdehyde dehydrogenase (AADH), converts lysine to aminoadipate (Fig. 2a). In a segregating population for the FLAG_*lkrsdh* locus, heterozygous, homozygous and wild-type plants were identified by genotyping, and subjected to LC-MS metabolic profiling after senescence induction (Fig. 2b, Supplementary Fig. 4). Acetyl-aminoadipate occurred at

105 the highest level in the heterozygous mutant, but was greatly reduced in the homozygous
106 mutant, suggesting that the ectopic accumulation of acetyl-aminoadipate in *BAR*-
107 containing plants is dependent on the activity of LKR/SDH in the lysine degradation
108 pathway in senescent leaves (Fig. 2a). By contrast, the relative abundance of acetyl-
109 tryptophan in the segregating population of FLAG_*lkrsdh* generally reflected the copy
110 number of the *BAR*-containing T-DNA transgene, with approximately 2-fold acetyl-
111 tryptophan level observed in the homozygotes compared to the heterozygotes (Fig. 2b).
112 Furthermore, acetyl-aminoadipate and acetyl-tryptophan levels were approximately 10-20
113 fold higher in senescent leaves than those in green leaves (Fig. 2b), which is likely due to
114 the increased availability of the corresponding free amino acids during senescence.
115 Consistent with these observations in leaves, ectopic accumulation of acetyl-
116 aminoadipate and acetyl-tryptophan was also observed in seeds of multiple *BAR*-
117 containing T-DNA mutant lines compared to the wild-type controls (Supplementary Fig.
118 5).

119 To shed light on the kinetic properties of BAR, we carried out pseudo-first-order
120 enzyme kinetic assays using recombinant BAR against several native and non-native
121 amino acid substrates (Fig. 3 and Supplementary Fig. 6). Similar to published data[1,3,17],
122 N-acetylation of phosphinothricin exhibits Michaelis-Menten kinetics with an apparent
123 K_m of approximately 132 μM (Fig. 3). Although BAR clearly showed N-acetyltransferase
124 activities toward aminoadipate and tryptophan, K_m values for these non-native substrates
125 could not be established, as both substrates reached solubility limit before reaching
126 saturation concentration for BAR. V_{max}/K_m values of BAR against aminoadipate and
127 tryptophan, which were inferred from Lineweaver-Burk plots, reveals that these two side

128 reactions are less favorable than the acetylation of phosphinothricin. BAR also exhibited
129 relatively higher catalytic activity toward aminoadipate than tryptophan *in vitro* (Fig. 3).

130 To reveal the structural basis for substrate selectivity and catalytic mechanism of
131 BAR that would enable structure-guided protein engineering, we determined the crystal
132 structures of the BAR/acetyl-CoA holocomplex and the BAR/CoA/phosphinothricin
133 ternary complex (see Supplementary Table 2 for data collection and refinement
134 statistics). Our refined structures revealed that BAR is an αβ protein harboring a globular
135 tertiary structure resembling the previously reported Gcn5-related N-acetyltransferase
136 (GNAT) structures (Supplementary Fig. 7)[18-21]. BAR crystalizes as a homodimer with
137 two active sites symmetrically distributed around the dimer interface inside a large open
138 cavity (Fig. 4a and Supplementary Fig. 8). The cofactor acetyl-CoA binds to a cleft
139 between α4 and α5 on the opposite side of the dimer interface with the acetyl group
140 pointing toward the catalytic center (Fig. 4a). Close examination of the BAR/acetyl-CoA
141 and BAR/CoA/phosphinothricin structures illuminates the catalytic mechanism of BAR
142 (Fig. 4b, 4c and Supplementary Fig. 9). Similar to other GNATs, BAR utilizes a
143 conserved catalytic Glu88 as a general base to deprotonate the amino group of
144 phosphinothricin through a water molecule as the proton shuttle (Fig. 4b, 4c, and
145 Supplementary Fig. 9)[21]. The deprotonated amino group then undergoes nucleophilic
146 attack on the carbonyl carbon of acetyl-CoA to produce a tetrahedral intermediate, which
147 is further stabilized by an oxyanion hole formed by a positively charged H137 and its
148 proton donor Y107 (Fig. 4c and Supplementary Fig. 9). Interestingly, the structural
149 feature underlying this oxyanion hole in BAR must have arisen independently from the
150 functionally analogous oxyanion hole previously described in the histone

acetyltransferase GCN5, featuring a backbone amide nitrogen instead[21]. In the final step of the catalytic cycle, coenzyme A is released from the tetrahedral intermediate as a leaving group to produce acetyl-phosphinothricin (Fig. 4c).

The BAR/CoA/phosphinothricin ternary structure also reveals active-site residues involved in phosphinothricin binding. Within each active site, the methylphosphoryl group of the substrate engages hydrophobic interactions with the surrounding F36, G127, and V161 from the same monomer, whereas the two phosphoryl oxygen atoms are coordinated by K78, R80, and Y83 from the β3-loop-α3 region of the neighboring monomer via a set of hydrogen bonds and electrostatic interactions (Fig. 4b). Furthermore, the amino acid group of phosphinothricin is properly positioned at the catalytic center by a hydrogen-bond network involving the backbone carbonyl group of V125 and the side chains of T90 and Y92 (Fig. 4b). Despite various attempts using co-crystallization and soaking techniques, structures of BAR containing aminoadipate or tryptophan could not be obtained, reflecting the low affinity of these nonspecific substrates to BAR. Simulated docking of these substrates within the active site of the BAR/CoA/phosphinothricin structure reveals fewer favorable interactions as well as potential steric clashes with the surrounding residues compared to phosphinothricin (Fig. 4d).

Site-directed mutagenesis followed by biochemical assays confirmed the roles of many active-site residues predicted by structural analysis (Fig. 4e and Supplementary Fig. 10). Mutating the catalytic E88 to alanine or glutamine greatly reduces the activity of BAR toward phosphinothricin and aminoadipate. Nevertheless, these mutants exhibit higher activity toward tryptophan than that of the wild-type enzyme at the substrate

concentration tested (Fig. 4e), suggesting that tryptophan may be deprotonated through an alternative mechanism independent of E88 and/or the first deprotonation step is not rate-limiting for BAR-catalyzed acetyl-tryptophan formation. H137A and Y107F mutants failed to yield sufficient soluble recombinant protein (Supplementary Fig. 10), preventing the role of the oxyanion hole in catalysis to be directly assessed. We thus probed this indirectly by mutating S133, a residue that forms a hydrogen bond with the imidazole ring π-nitrogen of H137 (Fig. 4b). The resulting S133A mutant exhibits completely abolished N-acetyltransferase activity toward the three tested substrates, suggesting an essential role of S133 in catalysis, likely through proper positioning of the imidazoline ring of the histidine within the oxyanion hole (Fig. 4e and Supplementary Fig. 9). Mutants affecting phosphinothricin-binding residues, including F36A, K78A, R80A, Y83F, Y92F, generally show significantly reduced activity toward phosphinothricin and aminoadipate, while K78A and Y83F display increased activity toward the more hydrophobic substrate tryptophan compared to the wild-type enzyme (Fig. 4e).

With the structural information of BAR in hand, we sought to engineer BAR through structure-guided mutagenesis to repress its undesired nonspecific activities toward aminoadipate and tryptophan while maintaining its native activity against phosphinothricin. We selected residue positions N35, Y73, T90, Y92, and V125 for targeted mutagenesis based on structural analysis as well as multiple sequence alignment containing BAR, PAT, and other closely related homologs from bacteria (Fig. 4b, 4d and Supplementary Fig. 11). A set of eleven mutants was first characterized *in vitro* (Fig. 4e), and eight of them were further tested in transgenic Arabidopsis (Fig. 4f and 4g). All eight BAR mutants confer phosphinothricin resistance in Arabidopsis T1 and T2 generations

(Fig. 4f, Supplementary Fig. 12-14). Metabolic profiling of these transgenic lines confirmed that mutations in select active-site residues of BAR can modulate the *in vivo* nonspecific activities of BAR toward aminoadipate and tryptophan (Fig. 4g). Notably, transgenic Arabidopsis plants containing Y73F, Y92F, N35T, N35D, T90A, V125L, or V125I BAR mutants display significantly reduced levels of acetyl-aminoadipate compared to plants containing wild-type BAR (Fig. 4g). Moreover, plants expressing Y73F, Y92F or T90A BAR mutants exhibit significantly reduced levels of both acetyl-aminoadipate and acetyl-tryptophan compared to plants containing wild-type BAR. These observed differences in acetyl-aminoadipate and acetyl-tryptophan levels are not due to BAR protein levels in transgenic plants (Supplementary Fig. 15), but are consistent with the altered catalytic activities of various BAR mutants measured *in vitro* (Fig. 4e and Supplementary Fig. 16). Subsequent analysis of N35T and Y92F revealed that both mutants exhibit compromised affinity toward native substrate phosphinothricin *in vitro* compared to wild-type BAR. However, N35T and Y92F retain largely unaltered catalytic speed *in vitro* and confer level of resistance to phosphinothricin *in planta* similar to that of wild-type BAR (Supplementary Fig. 16a and Supplementary Fig. 14). Furthermore, both mutants show more pronounced reduced catalytic activity toward one or both non-native substrates as compared to phosphinothricin (Supplementary Fig. 16).

Transgenic expression of enzymes catalyzing a variety of desirable biochemical reactions in heterologous hosts is a common strategy in both basic biological research and translational biotechnology. Prominent examples include reporter enzymes, such as firefly luciferase and β-glucuronidase, antibiotic/herbicide markers, such as aminoglycoside kinase that confers kanamycin resistance and BAR, and many enzymes

used for metabolic engineering purposes in microbes and higher eukaryotes[22]. Although enzymes are generally considered as perfected catalysts with superior substrate specificity and predictable catalytic mechanism, increasing evidences have raised awareness of the unpredictable behaviors of enzymes and their profound implication in natural and directed evolution of new enzymatic functions[23]. However, whether and how heterologous expression of a foreign enzyme would interfere with the native metabolic system remains an open question to be addressed on a case-by-case basis.

In this study, we discovered that transgenic expression of the herbicide-resistance enzyme BAR of bacterial origin indeed acetylate two endogenous amino acids, resulting in the ectopic accumulation of acetyl-aminoadipate and acetyl-tryptophan. While acetyl-tryptophan is a naturally occurring metabolite found in numerous plant species, including Arabidopsis, *Salsola collina*, *Glycine max*, *Solanum lycopersicum*, *Cocos nucifera*, and *Ginkgo biloba*[24,25], to the best of our knowledge, acetyl-aminoadipate has never been reported as an endogenous plant metabolite. Interestingly, in line with our findings, a recent study reported the ectopic accumulation of acetyl-aminoadipate in the flower tissue of a BAR-containing T-DNA mutant of Arabidopsis, which could not be rationalized by the mutated gene[26]. Despite the widespread use of BAR in GE crops[2,27] and the extensive testing and deregulation processes associated with this trait over the past few decades[1,3,17,28,29], such phenomenon was not reported elsewhere, probably due to technological limitation in metabolic profiling in the past. Studies have demonstrated indirect effects of BAR-containing transgenes in transgenic lines with high BAR expression, such as reduced fitness and modified amino acid levels, but without identifying their direct causes[5,6]. However, the implications of our findings about the

nonspecific activities of BAR on crop fitness and human/animal health are yet to be evaluated in future studies.

Our findings suggest that untargeted metabolomics analysis could be a useful methodology for future assessment of GE plants[7]. This study also provides solutions to reduce the nonspecific activities of BAR through structure-guided enzyme engineering so that its intended herbicide-degrading activity can be maximally insulated from the metabolome of the host.

CORRESPONDING AUTHORS

Correspondence to Jing-Ke Weng or Stefan Hörtensteiner.

ACKNOWLEDGMENTS

We thank D. M. Sabatini, G. R. Fink, N. Amrhein and E. Martinoia for helpful discussions. We thank J. M. Cheeseman for providing the phosphinothricin-resistant *Glycine max* line. We thank J. Varberg for providing the phosphinothricin-resistant *Brassica napus* line and M. Rahman for providing conventional *Brassica napus* lines. This work is based on research conducted at the Northeastern Collaborative Access Team (NE-CAT) beamlines, which are funded by the National Institute of General Medical Sciences from the National Institutes of Health (P41 GM103403). The Pilatus 6M detector on NE-CAT 24-ID-C beam line is funded by a NIH-ORIP HEI grant (S10 RR029205). This research used resources of the Advanced Photon Source, a U.S. Department of Energy (DOE) Office of Science User Facility operated for the DOE

265 Office of Science by Argonne National Laboratory under Contract No. DE-AC02-
266 06CH11357. This work was supported by the Swiss National Science Foundation (grant
267 31003A_149389 to S.H. and postdoctoral fellowship P2ZHP3_155258 to B.C.), the EU-
268 funded Plant Fellows program (S.A.), the Pew Scholar Program in the Biomedical
269 Sciences (J.K.W.) and the Searle Scholars Program (J.K.W.).
270

AUTHOR CONTRIBUTIONS

B.C., S.A., S.H. and J.K.W. designed experiments; B.C., R.H., L.G., R.F. and S.A. performed experiments; B.C., R.H., L.G. and J.K.W. analyzed data; B.C., S.H., S.A. and J.K.W. wrote the manuscript.

COMPETING FINANCIAL INTERESTS

B.C. and J.K.W. have filed a patent application on BAR and PAT mutants described in this paper that show altered acetyltransferase activity.

REFERENCES

1 Wehrmann, A., Van Vliet, A., Opsomer, C., Botterman, J. & Schulz, A. The similarities of *BAR* and *PAT* gene products make them equally applicable for plant engineers. *Nat. Biotechnol.* **14**, 1274-1278 (1996).

2 Duke, S. O. Taking stock of herbicide-resistant crops ten years after introduction. *Pest. Manag. Sci.* **61**, 211-218 (2005).

3 Thompson, C. J. *et al.* Characterization of the herbicide-resistance gene *BAR* from *Streptomyces hygroscopicus*. *EMBO J.* **6**, 2519-2523 (1987).

4 Wohlleben, W. *et al.* Nucleotide sequence of the phosphinothricin N-acetyltransferase gene from *Streptomyces viridochromogenes* Tü494 and its expression in *Nicotiana tabacum*. *Gene* **70**, 25-37 (1988).

5 Ren, Y. F. *et al.* A comparative proteomics approach to detect unintended effects in transgenic Arabidopsis. *J. Genet. Genomics* **36**, 629-639 (2009).

6 Brown, R. H., Raboy, V. & Bregitzer, P. Unintended consequences: high phosphinothricin acetyltransferase activity related to reduced fitness in barley. *In Vitro Cell. Dev. Biol. Plant* **49**, 240-247 (2013).

7 The National Academies. *Genetically Engineered Crops: Experiences and Prospects*. (National Academies Press, 2016).

8 Schenk, N. *et al.* The chlorophyllases *At*CLH1 and *At*CLH2 are not essential for senescence-related chlorophyll breakdown in *Arabidopsis thaliana*. *FEBS Lett.* **581**, 5517-5525 (2007).

9 Samson, F. *et al.* FLAGdb/FST: a database of mapped flanking insertion sites (FSTs) of *Arabidopsis thaliana* T-DNA transformants. *Nucleic Acids Res.* **30**, 94-97 (2002).

10 Sessions, A. *et al.* A high-throughput Arabidopsis reverse genetics system. *Plant Cell* **14**, 2985-2994 (2002).

11 Alonso, J. M. *et al.* Genome-wide insertional mutagenesis of *Arabidopsis thaliana*. *Science* **301**, 653-657 (2003).

12 Rosso, M. G. *et al.* An *Arabidopsis thaliana* T-DNA mutagenized population (GABI-Kat) for flanking sequence tag-based reverse genetics. *Plant Mol. Biol.* **53**, 247-259 (2003).

13 Soudry, E., Ulitzur, S. & Gepstein, S. Accumulation and remobilization of amino acids during senescence of detached and attached leaves: *in planta* analysis of tryptophan levels by recombinant luminescent bacteria. *J. Exp. Bot.* **56**, 695-702 (2005).

14 Hörtensteiner, S. & Feller, U. Nitrogen metabolism and remobilization during senescence. *J. Exp. Bot.* **53**, 927-937 (2002).

15 Arruda, P., Kemper, E. L., Papes, F. & Leite, A. Regulation of lysine catabolism in higher plants. *Trends Plant Sci.* **5**, 324-330 (2000).

16 Zhu, X., Tang, G., Granier, F., Bouchez, D. & Galili, G. A T-DNA insertion knockout of the bifunctional *LYSINE-KETOGLUTARATE REDUCTASE/SACCHAROPINE DEHYDROGENASE* gene elevates lysine levels in Arabidopsis seeds. *Plant Physiol.* **126**, 1539-1545 (2001).

17 Vinnemeier, J., DrogeLaser, W., Pistorius, E. K. & Broer, I. Purification and partial characterization of the *Streptomyces viridochromogenes* Tü494 phosphinothricin-N-acetyltransferase mediating resistance to the herbicide phosphinothricin in transgenic plants. *Z. Naturforsch. C.* **50**, 796-805 (1995).

18 Dyda, F., Klein, D. C. & Hickman, A. B. GCN5-related N-acetyltransferases: a structural overview. *Annu. Rev. Bioph. Biom.* **29**, 81-103 (2000).

19 Vetting, M. W. *et al.* Structure and functions of the GNAT superfamily of acetyltransferases. *Arch. Biochem. Biophys.* **433**, 212-226 (2005).

20 Srivastava, P. *et al.* Structural characterization of a GCN5-related N-acetyltransferase from *Staphylococcus aureus*. *PLoS ONE* **9** (2014).

21 Rojas, J. R. *et al.* Structure of Tetrahymena GCN5 bound to coenzyme A and a histone H3 peptide. *Nature* **401**, 93-98 (1999).

22 Woolston, B. M., Edgar, S. & Stephanopoulos, G. Metabolic engineering: past and future. *Annu. Rev. Chem. Biomol. Eng.* **4**, 259-288 (2013).

23 Weng, J. K. & Noel, J. P. The remarkable pliability and promiscuity of specialized metabolism. *Cold Spring Harb. Symp. Quant. Biol.* **77**, 309-320 (2012).

24 Jin, Y.-S. *et al.* Chemical and biologically active constituents of *Salsola collina*. *Chem. Nat. Compd.* **47**, 257-260 (2011).
25 Yu, P., Hegeman, A. D. & Cohen, J. D. A facile means for the identification of indolic compounds from plant tissues. *Plant J.* **79**, 1065-1075 (2014).
26 Bruckhoff, V. *et al.* Functional characterization of CYP94-genes and identification of a novel jasmonate catabolite in flowers. *PLoS One* **11**, e0159875 (2016).
27 Green, J. M. & Owen, M. D. Herbicide-resistant crops: utilities and limitations for herbicide-resistant weed management. *J. Agric. Food Chem.* **59**, 5819-5829 (2011).
28 Herouet, C. *et al.* Safety evaluation of the phosphinothricin acetyltransferase proteins encoded by the *PAT* and *BAR* sequences that confer tolerance to glufosinate-ammonium herbicide in transgenic plants. *Regul. Toxicol. Pharm.* **41**, 134-149 (2005).
29 Dan, Y. *Plant transformation technology revolution in last three decades: historical technology developments*. (Bentham Science Publishers, 2012).
30 Song, W. Y., Choi, K. S., Alexis de, A., Martinoia, E. & Lee, Y. Brassica juncea plant cadmium resistance 1 protein (BjPCR1) facilitates the radial transport of calcium in the root. *Proc. Natl. Acad. Sci. U.S.A.* **108**, 19808-19813 (2011).
31 Foetzki, A. *et al.* Surveying of pollen-mediated crop-to-crop gene flow from a wheat field trial as a biosafety measure. *GM Crops Food* **3**, 115-122 (2012).
32 Czechowski, T., Stitt, M., Altmann, T., Udvardi, M. K. & Scheible, W. R. Genome-wide identification and testing of superior reference genes for transcript normalization in Arabidopsis. *Plant Physiol.* **139**, 5-17 (2005).
33 Chambers, M. C. *et al.* A cross-platform toolkit for mass spectrometry and proteomics. *Nat. Biotechnol.* **30**, 918-920 (2012).
34 Gowda, H. *et al.* Interactive XCMS Online: simplifying advanced metabolomic data processing and subsequent statistical analyses. *Anal. Chem.* **86**, 6931-6939 (2014).
35 Smith, C. A. *et al.* METLIN: a metabolite mass spectral database. *Ther. Drug Monit.* **27**, 747-751 (2005).
36 Tropea, J. E., Cherry, S. & Waugh, D. S. Expression and purification of soluble His(6)-tagged TEV protease. *Methods Mol. Biol.* **498**, 297-307 (2009).
37 Battye, T. G., Kontogiannis, L., Johnson, O., Powell, H. R. & Leslie, A. G. iMOSFLM: a new graphical interface for diffraction-image processing with MOSFLM. *Acta Crystallogr. D* **67**, 271-281 (2011).
38 Evans, P. Scaling and assessment of data quality. *Acta Crystallogr. D* **62**, 72-82 (2006).
39 Adams, P. D. *et al.* PHENIX: a comprehensive Python-based system for macromolecular structure solution. *Acta Crystallogr. D* **66**, 213-221 (2010).
40 Emsley, P. & Cowtan, K. Coot: model-building tools for molecular graphics. *Acta Crystallogr. D* **60**, 2126-2132 (2004).
41 Goldstein, A. L. & McCusker, J. H. Three new dominant drug resistance cassettes for gene disruption in *Saccharomyces cerevisiae*. *Yeast* **15**, 1541-1553 (1999).
42 Engler, C. *et al.* A Golden Gate modular cloning toolbox for plants. *ACS Synth. Biol.* (2014).
43 Clough, S. J. & Bent, A. F. Floral dip: a simplified method for Agrobacterium-mediated transformation of *Arabidopsis thaliana*. *Plant J.* **16**, 735-743 (1998).
44 Schelbert, S. *et al.* Pheophytin pheophorbide hydrolase (pheophytinase) is involved in chlorophyll breakdown during leaf senescence in Arabidopsis. *Plant Cell* **21**, 767-785 (2009).
45 Christ, B. *et al.* MES16, a member of the methylesterase protein family, specifically demethylates fluorescent chlorophyll catabolites during chlorophyll breakdown in Arabidopsis. *Plant Physiol.* **158**, 628-641 (2012).
46 Guyer, L. *Characterization of dephytylation and dechelation, two early steps of chlorophyll breakdown in leaves and fruits* PhD thesis, Zurich, (2015).
47 Christ, B. *et al.* Cytochrome P450 CYP89A9 is involved in the formation of major chlorophyll catabolites during leaf senescence in Arabidopsis. *Plant Cell* **25**, 1868-1880 (2013).
48 Perez-Perez, J. M. *et al.* Functional redundancy and divergence within the Arabidopsis RETICULATA-RELATED gene family. *Plant Physiol.* **162**, 589-603 (2013).
49 Christ, B. *Chlorophyll breakdown: modifications of colorless chlorophyll catabolites* PhD thesis, Zurich, (2013).

50 Zufferey, M. *et al.* The novel chloroplast outer membrane kinase KOC1 is a required component of the plastid protein import machinery. *J. Biol. Chem.* **292**, 6952-6964 (2017).
51 Pulido, P., Llamas, E. & Rodriguez-Concepcion, M. Both Hsp70 chaperone and Clp protease plastidial systems are required for protection against oxidative stress. *Plant Signal. Behav.* **12** (2017).
52 Waterhouse, A. M., Procter, J. B., Martin, D. M., Clamp, M. & Barton, G. J. Jalview Version 2 - a multiple sequence alignment editor and analysis workbench. *Bioinformatics* **25**, 1189-1191 (2009).

FIGURE LEGENDS

Figure 1 | Accumulation of acetyl-aminoadipate and acetyl-tryptophan in senescent leaves of Arabidopsis carrying the BAR transgene. **a**, Metabolite profiles of senescent leaves from Wassilewskija (Ws) and *clh2-1* (FLAG-1), displayed as base peak chromatograms (BPC), reveal the ectopic accumulation of acetyl-aminoadipate (**1**) and acetyl-tryptophan (**2**). BPC traces of four biological replicates are displayed. **b**, Comparative levels of acetyl-aminoadipate and acetyl-tryptophan in Arabidopsis mutants from different insertional mutant collections that contain either BAR (SAIL and FLAG) or alternative selection marker genes (SALK (*NTPII*, kanamycin resistance) and GABI (*SULI*, sulfadiazine resistance)). Error bars, mean ± s.d. (n = 3 biological replicates). This experiment was repeated at least three times with similar results. See Supplementary Fig. 2 for absolute quantification. a.u., arbitrary unit; FW, fresh weight; n.d., not detected

Figure 2 | BAR-dependent accumulation of acetyl-aminoadipate and acetyl-tryptophan is linked to nitrogen remobilization during senescence. **a**, Aminoadipate is derived from the lysine degradation pathway in plants, which can be metabolized by BAR as a nonspecific substrate. **b**, Comparative levels of acetyl-aminoadipate and acetyl-tryptophan in green and senescent leaves from the heterozygous (He) and homozygous (Ho) FLAG_*lkrsdh* mutant, harboring a BAR-containing T-DNA that abolishes the

418 Arabidopsis *LKR/SDH* gene. Error bars, mean ± s.d. (n = 4 biological replicates). a.u.,
419 arbitrary unit; n.d., not detected; Ws, Wassilewskija wild-type plants.
420
421 **Figure 3 | In vitro enzyme kinetic assays of BAR against native and non-native**
422 **substrates.** An apparent K_M value of 132 ± 19.2 μM was obtained for phosphinothricin,
423 similar to previously published data[1,3,17]. V_{max}, k_{cat}, k_{cat}/K_m and V_{max}/K_m values for
424 phosphinothricin are also indicated, as well V_{max}/K_m values for aminoadipate and
425 tryptophan (estimated from Lineweaver-Burk plots). Aminoadipate and tryptophan are in
426 vitro substrates of BAR but both substrates reached solubility limit before reaching
427 saturation concentration for BAR. Negative controls (open circles) were performed in
428 absence of BAR at the highest substrate concentration tested (20 mM).
429
430 **Figure 4 | Structural basis for amino acid N-acetylation catalyzed by BAR and**
431 **structure-guided engineering of BAR with reduced nonspecific activities. a**, Cartoon
432 representation of BAR homodimer in complex with phosphinothricin and CoA. Two
433 monomers of the dimer are colored in blue and yellow respectively. **b**, Close-up view of
434 the BAR active site. The |2Fo-Fc| omit electron density map (contoured at 3.0 σ) is
435 shown for phosphinothricin. **c**, Proposed catalytic mechanism of BAR. **d**, Docking of
436 tryptophan and aminoadipate within the BAR active site reveals reduced favorable
437 contacts compared to phosphinothricin. **e**, Enzyme activity assays using purified BAR
438 mutant proteins against phosphinothricin (0.2mM), aminoadipate (1 mM) and tryptophan
439 (1 mM). Wild-type BAR (WT BAR) and PAT from Streptomyces viridochromogenes
440 were also examined as controls. Assays were terminated during the initial linear rate of

product formation. The relative amount of product formed by each BAR mutant was normalized to WT BAR for each substrate (value of 1). Error bars, mean ± s.d. (n = 3 technical replicates). **f**, Photographs of Arabidopsis T1 lines transformed with select BAR mutants 10 days after phosphinothricin treatment (see also Supplementary Fig. 12-14). Scale bar = 0.3 cm. **g**, Comparative levels of acetyl-aminoadipate and acetyl-tryptophan in phosphinothricin-resistant T2 Arabidopsis plants transformed with selected BAR mutants. Error bars, mean ± s.d. (n = 5-6 biological replicates: Y73F (6), Y92F (6), N35T (5), N35S (5), T90A (6), V125T (5), V125L (6), V125I (6), WT BAR (5), PAT (5)). Significance levels were indicated based on one-way ANOVA with Dunnett's test for multiple comparisons to WT BAR. a, p-value < 0.1; b, p-value < 0.05; c, p-value < 0.01; a.u., arbitrary unit.

Materials and Methods

Plant materials

Arabidopsis (*Arabidopsis thaliana*) Columbia-0 (Col-0) and Wassilewskija (Ws) were used as wild types. T-DNA insertion lines were from the following collections: SALK lines[11]: SALK_130606 (SALK_1), SALK_051823C (SALK_2), SALK_110649 (SALK_3); SAIL lines[10]: SAIL_1165_B02 (SAIL_1), SAIL_503_C03 (SAIL_2), SAIL_1235_D10 (SAIL_3); GABI lines[12]: GABI_453E01 (GABI_1), GABI_833F02 (GABI_2), GABI_453A08 (GABI_3); FLAG lines[9]: FLAG_076H05 (*clh2-1*[8]; FLAG_1), FLAG_271B02 (FLAG_2), FLAG_495A09 (FLAG_3), FLAG_271B12 (FLAG_*lkrsdh*). SALK, SAIL and GABI lines were obtained from the European Arabidopsis Stock Center (http://arabidopsis.info/). The FLAG lines were obtained from the INRA

464 Versailles Arabidopsis Stock Center (http://publiclines.versailles.inra.fr/). Homozygous
465 (and heterozygous for FLAG_*lkrsdh*) plants were identified by PCR using T-DNA- and
466 gene-specific primers.

467 Arabidopsis T-DNA lines used for untargeted metabolomics and relative
468 quantification of acetyl-aminoadipate and acetyl-tryptophan were grown on soil under a
469 12-h-light/12-h-dark photoperiod with fluorescent light of 80 to 120 µmol photons m^{-2} s^{-1}
470 at 22°C and 60% relative humidity. For senescence induction, leaves from 5-week-old
471 plants were excised and incubated in permanent darkness on wet filter paper for 8 d at
472 ambient temperature. Transgenic Arabidopsis lines transformed with BAR mutants and
473 Arabidopsis T-DNA lines used for absolute quantification of acetyl-aminoadipate and
474 acetyl-tryptophan were grown on soil under a 16-h-light/8-h-dark photoperiod with
475 fluorescent light of 80 to 120 µmol photons m^{-2} s^{-1} at 22°C and 60% relative humidity.
476 For senescence induction, leaves from phosphinothricin-resistant, 4-week-old plants were
477 excised and incubated in permanent darkness on wet filter paper for 6 d at ambient
478 temperature. For measuring the expression of LKR/SDH in FLAG_271B12, seedlings
479 were grown for 7 days on ½ Murashige and Skoog (MS) plates containing 1% sucrose.

480 Phosphinothricin-resistant *Glycine max* (Liberty Link trait A2704-12, 283 Morril
481 MC-116, Credenz CZ 3841 LL, Bayer CropScience), wild-type (non-isogenic) *Glycine*
482 *max* (Chiba Green; High Mowing Organic Seed), lines were grown on soil under a 16-h-
483 light/8-h-dark photoperiod with fluorescent light of 80 to 120 µmol photons m^{-2} s^{-1} at
484 22°C and 60% relative humidity. Green and senescent leaf samples were collected from
485 40-days old plants. This experiment was repeated once with similar results.

Phosphinothricin-resistant *Brassica napus* (Liberty Link trait L252, Bayer CropScience) and wild-type (non-isogenic) *Brassica napus* (NDC-E12131, NDC-E13285 and NDC-E12027) lines were grown on soil under a 16-h-light/8-h-dark photoperiod with fluorescent light of 80 to 120 μmol photons m^{-2} s^{-1} at 22°C and 60% relative humidity. For senescence induction, fully developed cotyledons were excised and incubated in permanent darkness on wet filter paper for 5-7 days at ambient temperature. This experiment was done once.

Wild-type (isogenic) and phosphinothricin-resistant *Brassica juncea*[30] were grown on soil under a 16-h-light/8-h-dark photoperiod with fluorescent light of 80 to 120 μmol photons m^{-2} s^{-1} at 22°C and 60% relative humidity. For senescence induction, fully developed cotyledons were excised and incubated in permanent darkness on wet filter paper for 5-7 d at ambient temperature.

Wild-type (isogenic) and phosphinothricin-resistant *Triticum aestivum*[31] were grown on soil under a 16-h-light/8-h-dark photoperiod with fluorescent light of 80 to 120 μmol photons m^{-2} s^{-1} at 22°C and 60% relative humidity. For senescence induction, leaves were excised and incubated in permanent darkness on wet filter paper for 5-7 d at ambient temperature.

RNA Isolation and qRT-PCR

Total RNA was extracted using a Qiagen RNeasy Plant Mini Kit according to manufacturer's instructions (DNase treatment was performed on-column). The concentration and purity of RNA were determined by absorbance at 260/280 nm. First-strand cDNA was synthesized from 1 μg of RNA using SuperScript III Reverse

Transcriptase with Oligo dT primers (Thermo Scientific). Reactions were run on a QuantStudio 6 system machine (Thermo Scientific) using Sybr Green Master Mix (Thermo Scientific) using primer listed in Supplementary Fig. 4 and Supplementary Table 3. Gene expression values were calculated using Ct values and normalized using the reference gene At1g13320[32].

Metabolite extraction

Arabidopsis and *Brassica napus* samples were collected in 2 mL Eppendorf tubes containing 500 µL of 1.5 mm glass beads, weighted and snap-frozen in liquid nitrogen. The frozen samples were ground using a MM300 Mixer Mill (Retsch) at 30 Hz for 5 min and stored at -80°C until further processing. *Glycine max* samples were snap-frozen in liquid nitrogen and ground with a mortar and pestle. Metabolites were extracted using 5-10 (for leaf samples) or 10 -50 volumes (for seed samples; w/v) of ice-cold extraction buffer (80% methanol, 20% water, 0.1% formic acid (v/v/v)). Extracts were homogenized at 30 Hz for 5 min and centrifuged (14,000-16,000 g, 4°C). After re-centrifugation, supernatants were transferred to LC vials and analyzed by LC-MS.

LC-MS analysis of Arabidopsis T-DNA mutants, *Brassica juncea* and *Triticum aestivum* (untargeted metabolomics and relative quantification of acetyl-aminoadipate and acetyl-tryptophan)

The LC-MS instrument was composed of an Ultimate 3000 Rapid Separation LC system (Thermo Scientific) coupled to a Bruker Compact ESI-Q-TOF (Bruker Daltonics). The reverse-phase chromatography system consisted of an 150 mm C18

column (ACQUITY UPLC™ BEH, 1.7 µm, 2.1 x 150 mm, Waters), which was developed using LC-MS solvents (Chemie Brunschwig) with a gradient (flow rate of 0.3 mL min^{-1}) of solvent B (acetonitrile with 0.1% (v/v) formic acid) in solvent A (water with 0.1% (v/v) formic acid) as follows (all (v/v)): 5% for 0.5 min, 5% to 100% in 11.5 min, 100% for 4 min, 100% to 5% in 1 min and 5% for 1 min. Electrospray ionization (ESI) source conditions were set as follows: gas temperature, 220°C; drying gas, 9 L min^{-1}; nebulizer, 2.2 BAR; capillary voltage, 4500 V; end plate offset, 500 V. Tuning conditions were set as follows: funnel 1 RF, 250 Vpp; funnel 2 RF, 150 Vpp; isCID energy, 0 eV; hexapole RF, 50 Vpp; quadrupole ion energy, 3.0 eV; quadrupole low mass, 90 m/z; collision cell, 6 eV; pre-pulse storage time, 3 µs. The instrument was set to acquire over the m/z range 50-1300, with an acquisition rate of 4 spectra s^{-1}. Conditions for MS^2 of automatically selected precursors (data-dependent MS^2) were set as follows: threshold, 1000 counts; active smart exclusion (5x); active exclusion (exclude after 3 spectra, release after 0.2 min, reconsider precursor if current intensity/previous intensity is ≥5); number of precursors, 3; active stepping (basic mode, timing 50%-50%, collision RF from 350 to 450 Vpp, transfer time from 65 to 80 µs, collision energy from 80 to 120%). All data were recalibrated internally using pre-run injection of sodium formate (10 mM sodium hydroxide in 0.2% formic acid, 49.8% water, 50% isopropanol (v/v/v)). After data recalibration using DataAnalysis (version 4.2, Bruker Daltonics) and data conversion to mzXML format using ProteoWizard MSConvert[33], metabolite features detected in Ws and FLAG_076H05 (senescent leaves, four replicates) were aligned according to retention time and relatively quantified using XCMS online[34] (pairwise comparison using XCMS online pre-set parameters “UPLC/Bruker Q-TOF”). Up-regulated features in

555 FLAG_076H05 were identified at retention times of 2.8 min (labeled as "1" in Fig. 1a,
556 m/z 204.086 (fold change ≥10, p-value ≤0.005, intensity threshold 800,000)) and 6.5 min
557 (labeled as "2" in Fig. 1a, m/z 247.108 (fold change ≥10, p-value ≤0.005, intensity
558 threshold 100,000)) and further characterized as ions derived from N-acetyl-D/L-
559 aminoadipate and N-acetyl-D/L-tryptophan, respectively, by database searches in
560 METLIN[35] using MS and MS^2 spectra. Relative quantification of acetyl-aminoadipate
561 and acetyl-tryptophan in Arabidopsis mutants from different insertion mutant collections
562 was carried out by QuantAnalysis (version 2.2, Bruker Daltonics) using extracted ion
563 chromatogram (EIC) traces ($[M+H]^+$). Metabolomics data generated in this study have
564 been uploaded to the EBI MetaboLights database (http://www.ebi.ac.uk/metabolights/)
565 with the following accession number (MTBLS553).
566

567 **Absolute quantification of free amino acids in senescent leaves of Arabidopsis T-**
568 **DNA mutants**

569 The LC-MS instrument was composed of an Ultimate 3000 Rapid Separation LC system
570 (Thermo Scientific) coupled to a Q-Exactive mass spectrometer (Thermo Scientific). The
571 HILIC chromatography system consisted of SeQuant ZIC-pHILIC Polymeric column
572 (2.1 × 150 mm, 5 μM, EMD Millipore), which was developed using Optima™ LC/MS
573 solvents (Fisher Chemical) with a gradient (flow rate of 0.15 mL min^{-1}) of solvent B
574 (acetonitrile) in solvent A (20 mM ammonium carbonate, 0.1% ammonium hydroxide) as
575 follows (all (v/v)): 80% to 20% in 20 min, 80% to 20% in 0.5 min and 80% for 7.5 min.

576 The mass spectrometer was operated in full-scan (resolution, 70'0000; AGC
577 target, 1e6; Maximum IT, 20ms) polarity switch mode with the spray voltage set to +/-

3.0 kV, the heated capillary held at 275C, and the HESI probe held at 350C. Seventeen labeled amino acids (MSK-A2-1.2, Cambridge Isotope Laboratories) were added to the extraction solvent (80% methanol, 20% water) and used as internal standards. Standard curves were performed for each 25 amino acids. Acetyl-aminoadipate was synthesized using recombinant BAR as described below and all 24 other amino acids were purchased from Sigma-Aldrich. Data analysis was performed with Xcalibur (Thermo Scientific). Note that values for a few amino acids are shown as relative levels in Supplementary Fig. 2 because their concentrations in some samples were more than 10-fold higher than the highest concentration of the standard.

Absolute quantification of acetyl-aminoadipate and acetyl-tryptophan in seeds of Arabidopsis T-DNA mutants and various tissues of *Glycine max* and *Brassica napus*

Metabolites were extracted as described above and then analyzed on an Ultimate 3000 Rapid Separation LC system (Thermo Scientific) coupled to a TSQ Quantum Access MAX triple-quadrupole mass spectrometer (Thermo Scientific). The reverse-phase chromatography system consisted of an 150 mm C18 column (Kinetex 2.6 µm silica core shell C18 100Å pore, Phenomenex) which was developed using Optima™ LC/MS solvents (Fisher Chemical) with a gradient (flow rate of 0.6 mL min^{-1}) of solvent B (acetonitrile with 0.1% (v/v) formic acid) in solvent A (water with 0.1% (v/v) formic acid) as follows (all (v/v)): 2% for 3 min, 2% to 99% in 9 min, 99% for 4 min, 99% to 2% in 1 min and 2% for 1 min. The mass spectrometer was configured to perform two selected-reaction-monitoring scans, each for 0.5 seconds, for acetyl-aminoadipate and acetyl-tryptophan. The m/z resolution of Q1 was set to 0.4 FWHM, the nitrogen collision

gas pressure of Q2 was set to 1.5 mTorr, and the Q3 scan width was set to 0.500 m/z in both cases. Selected reaction monitoring for acetyl-aminoadipate was as follows: precursor ion selection at 204.086 m/z on positive ion mode, fragmentation at 10 V, and product ion selection at 144.065 m/z. Selected reaction monitoring for acetyl-tryptophan was as follows: precursor ion selection at 247.107 m/z on positive ion mode, fragmentation at 20 V, and product ion selection at 188.070 m/z. Acetyl-aminoadipate was synthesized using recombinant BAR as described below and used as standard. Pure acetyl-tryptophan was purchased from Sigma-Aldrich.

Heterologous expression of wild-type BAR and activity determination

The BAR coding sequence was amplified by PCR (KaPa HiFi HotStart polymerase; KaPa Biosystems) from genomic DNA extracted from homozygous plants of the SAIL line SAIL_1165_B02 using primers SAIL_BAR_F_pPROEX and SAIL_BAR_R_pPROEX (see Table S3) and then cloned into pProEX Hta (Invitrogen) via *Eco*RI and *Hin*dIII resulting in a 6xHis-BAR fusion construct.

6xHis-tagged BAR protein was expressed in *E. coli* BL21(DE3) grown in Terrific Broth medium. At an optical density at 600 nm of 0.6, protein expression was induced with 1.0 mM IPTG and cells were grown at 37°C for 2.5 h. Cells from 1 L culture were harvested by centrifugation and resuspended in 25 mL binding buffer (50 mM Tris-HCl pH 8, 500 mM NaCl, 30 mM imidazole). All the following steps were carried out at 4°C. Cell lysis was performed using a microfluidizer (HC-8000, Microfluidics). The lysate was centrifuged (16,000 g) for 20 min, and the 6xHis-tagged BAR protein was purified by metal affinity (5-ml HisTrap HP column, GE Healthcare) and size-exclusion

chromatography (HiLoad 16/600 Superdex 200 pg, GE Healthcare) using an ÄKTA Pure FPLC system (GE Healthcare). The 6xHis-TEV tag was removed from BAR prior to size-exclusion chromatography by overnight incubation with 1 µg of 6xHis-TEV protease[36] per 10 µg protein in 50 mM Tris-HCl pH 8, 500 mM NaCl, 1 mM dithiothreitol, followed passage through HisTrap HP column. Purified recombinant BAR was dialyzed in storage buffer (12.5 mM Tris-HCl pH 8, 50 mM NaCl, 2 mM dithiothreitol) and concentrated to 13 mg/mL using an ultra-centrifugal filter (10,000 Da MWCO, Amicon EMD Millipore). The purity of recombinant BAR was assessed by SDS-PAGE (Supplementary Fig. 6a). Purified BAR was aliquoted, snap-frozen in liquid nitrogen and stored at -80°C until further use.

Enzyme assays were carried out in 2 mM Tris-HCl pH 8 and 10 mM acetyl-CoA (Sigma-Aldrich; final volume 25 µl). Before determining the kinetics of BAR with different substrates, time-dependent activity of the purified protein was tested at substrate concentrations of 500 µM L-phosphinothricin (glufosinate ammonium, considered as a 1:1 mixture of L- and D- enantiomers; Sigma-Aldrich) or 1 mM (L-aminoadipate and L-tryptophan; Sigma-Aldrich). Reactions were initiated by the addition of purified BAR at 0.26 µM (assays with L-phosphinothricin) or 150 µM (assays with aminoadipate or tryptophan) and incubated at 25°C for the indicated times (Supplementary Fig.3 b-d). Reactions were stopped by the addition of four volumes of 10% water, 90% acetonitrile (v/v), 5 mM ammonium formate pH 3. Likewise, substrate concentration-dependence was determined by incubating assays for 25 min (assays with L-phosphinothricin), 3 h (assays with aminoadipate) or 7 h (assays with tryptophan; Fig. 3). Stock solutions of aminoadipate and tryptophan at 60 mM were made in 2 mM Tris-HCl pH 8 supplemented

with 1 mM N-nonyl β-D-glucopyranoside and substrate concentration-dependence assays employing these two substrates contained 0.33 mM N-nonyl β-D-glucopyranoside. Control assays (Fig. 3) were performed with aminoadipate and tryptophan at 20 mM, but in the absence of BAR.

The assays were analyzed on an Ultimate 3000 Rapid Separation LC system (Thermo Scientific) coupled to a TSQ Quantum Access MAX triple-quadrupole mass spectrometer (Thermo Scientific). Assays on phosphinothricin were analyzed as follows. The normal-phase chromatography system consisted of an 150 mm HILIC column (Kinetex 2.6 µm silica core shell HILIC 100Å pore, Phenomenex), which was developed using Optima™ LC/MS solvents (Fisher Chemical) with a gradient (flow rate of 0.8 mL min^{-1}) of solvent B (50% water, 50% acetonitrile (v/v), 5 mM ammonium formate pH 3) in solvent A (10% water, 90% acetonitrile (v/v), 5 mM ammonium formate pH 3) as follows (all (v/v)): 0% for 2 min, 0% to 70% in 10 min, 70% to 100% in 30 sec, 100% for 90 sec, 100% to 0% in 30 sec and 0% for 3.5 min. The mass spectrometer was configured to perform selected-ion-monitoring scans of 0.5 seconds using Q3 (center mass m/z: 224.068, scan width 1.0 m/z, scan time 0.5 sec). Assays on aminoadipate and tryptophan were analyzed as described above for the absolute quantification of acetyl-aminoadipate and acetyl-tryptophan in planta. Product formation was quantified using standards synthesized using recombinant BAR (acetyl-phosphinothricin and acetyl-aminoadipate) or commercially available (acetyl-tryptophan, Sigma-Aldrich). K_m and V_{max} value for phosphinothricin were inferred using the Michaelis-Menten kinetics nonlinear regression function under Prism 6 (GraphPad).

X-ray crystallography

Purified BAR protein was incubated with 1 mM acetyl-CoA for >2 hour prior to setting crystal trays. Crystals of BAR were obtained after 3 days at 20 °C in hanging drops containing 1 μL of protein solution (7.5 mg/mL) and 1 μL of reservoir solution (0.18 M calcium acetate, 0.1 M Tris-HCl pH 7, 18% (w/v) PEG 3000, 0.2% (v/v) N-nonyl β-D-glucopyranoside, 1 mM acetyl-CoA). Several crystals were soaked in reservoir solution supplemented with 30 mM L-phosphinothricin for 30-60 min before freezing. Crystals were frozen in reservoir solution supplemented with 15% (v/v) ethylene glycol. Acetylation of phosphinothricin occurred during soaking as no density for the acetyl group of acetyl-CoA was observed in the BAR/CoA/phosphinothricin ternary complex.

X-ray diffraction data were collected on the 24-ID-C beam line of the Structural Biology Center at the Advanced Photon Source (Argonne National Laboratory) equipped with a Pixel Array Detector (Pilatus-6MF). Diffraction intensities were indexed, integrated, and scaled with the iMosflm[37] and SCALA[38] programs. Initial phases were determined by molecular replacement using Phaser under Phenix[39]. The search model was an ensemble model generated with Ensembler using 8 protein structures homologous to BAR (PBD codes and % identity to BAR: 2JLM (28%), 3DR8 (35%), 4J3G (31%), 4JXQ (33%), 4MBU (30%), 1VHS (30%), 1YR0 (29%) and 1YVO (35%)). Subsequent structural building and refinements utilized Phenix programs (TSL was used in early rounds of refinement)[39]. Coot was used for graphical map inspection and manual rebuilding of atomic models[40]. Crystallographic calculations were performed using Phenix. Molecular graphics were produced with the program PyMol.

693 **Heterologous expression of BAR mutants and activity determination**

694 Single amino acid mutants of BAR were generated using the QuikChange II site-
695 directed mutagenesis kit (Agilent Technologies) and 6xHis-BAR in pProEX Hta as
696 template (see Supplementary Table 3 for primer sequences). PAT from *Streptomyces*
697 *viridochromogenes* was amplified using primers BAC0327 and BAC0328 from pAG31
698 vector [41] (Addgene 35124) and cloned into *Bam*HI/*Hin*dIII-linearized pProEX Hta by
699 Gibson assembly (New England Biolabs). Wild-type 6xHis-BAR, 6xHis-BAR mutants
700 and 6xHis-PAT were expressed in *E. coli* BL21(DE3) grown in Terrific Broth medium.
701 At an optical density at 600 nm of 0.6, protein expression was induced with 1.0 mM
702 IPTG and cells were grown at 37°C for 2.5 h. Cells from a 150 mL cultures were
703 harvested by centrifugation, lysed using B-PER™ Bacterial Protein Extraction Reagent
704 (Thermo Scientific) and purified by metal affinity using Ni-NTA Agarose (Qiagen).
705 Purified recombinant proteins were concentrated and buffer-exchanged using storage
706 buffer (10 mM Tris-HCl pH 8.0, 0.2 M NaCl, 10% (v/v) glycerol, 1 mM dithiothreitol)
707 and ultra-centrifugal filters (10,000 Da MWCO, Amicon EMD Millipore). The purity of
708 the recombinant proteins was assessed by SDS-PAGE. Final protein concentrations were
709 determined and normalized using a NanoDrop 2000 UV-VIS spectrometer (extinction
710 coefficient: 43430 M^{-1} cm^{-1}, Thermo Scientific).

711 Enzyme assays for comparing the relative activity of the purified BAR mutants
712 were carried out in 2 mM Tris-HCl pH 8 and 5 mM acetyl-CoA (Sigma-Aldrich) (final
713 reaction volume 12 µL). Reactions were initiated by the addition of purified recombinant
714 protein at 0.2 µM (assays with L-phosphinothricin at 0.2 mM) or 150 µM (assays with
715 aminoadipate or tryptophan at 1 mM) and incubated at 25°C for 15 min

716 (phosphinothricin), 165 min (aminoadipate), or 330 min (L-tryptophan). Substrate
717 concentration-dependences toward phosphinothricin, aminoadipate and tryptophan were
718 determined for the BAR mutants Y92F and N35T in 2 mM Tris-HCl pH 8 and 10 mM
719 acetyl-CoA (Sigma-Aldrich). Note that assays on aminoadipate and tryptophan were
720 supplemented with 0.33 mM of N-nonyl β-D-glucopyranoside (see also above).
721 Reactions were stopped by the addition of four volumes of 10% water, 90% acetonitrile
722 (v/v), 5 mM ammonium formate pH 3, centrifuged for 2 min (14,000-16,000 g), and
723 transferred to LC vials.

724 The assays were analyzed on an Ultimate 3000 Rapid Separation LC system
725 (Thermo Scientific) coupled to a TSQ Quantum Access MAX triple-quadrupole mass
726 spectrometer (Thermo Scientific). Assays on phosphinothricin were analyzed as
727 described above. Assays on aminoadipate were analyzed as follows. The reverse-phase
728 chromatography system consisted of an 150 mm C18 column (Kinetex 2.6 µm silica core
729 shell C18 100Å pore, Phenomenex), which was developed using Optima™ LC/MS
730 solvents (Fisher Chemical) with a gradient (flow rate of 0.6 mL min^{-1}) of solvent B
731 (acetonitrile with 0.1% (v/v) formic acid) in solvent A (water with 0.1% (v/v) formic
732 acid) as follows (all v/v): 1% for 2 min, 1% to 30% in 9 min, 30% to 99% in 30 sec, 99%
733 for 30 sec, 99% to 1% in 1 min and 1% for 2 min. The mass spectrometer was configured
734 to perform selected-ion-monitoring scans of 0.5 seconds using Q3 (center mass m/z:
735 204.086, scan width 0.5 m/z, scan time 0.5 sec). Assays on tryptophan were analyzed as
736 follow: the reverse-phase chromatography system consisted of an 150 mm C18 column
737 (Kinetex 2.6 µm silica core shell C18 100Å pore, Phenomenex) which was developed
738 using Optima™ LC/MS solvents (Fisher Chemical) with a gradient (flow rate of 0.7 mL

739 min^{-1}) of solvent B (acetonitrile with 0.1% (v/v) formic acid) in solvent A (water with
740 0.1% (v/v) formic acid) as follows (all v/v): 5% for 1 min, 5% to 99% in 9 min, 99% for
741 2 min, 99% to 5% in 2 min and 5% for 1 min. The mass spectrometer was configured to
742 perform selected-ion-monitoring scans of 0.5 seconds using Q3 (center mass m/z:
743 247.108, scan width 0.5 m/z, scan time 0.5 sec).

744

745 **Analysis of BAR mutants in planta**

746 Wild-type BAR from *Streptomyces hygroscopicus*, selected BAR mutants and wild-type
747 PAT from *Streptomyces viridochromogenes* were amplified by PCR (Phusion
748 polymerase; New England Biolabs) from pProEX Hta clones (see above) using primers
749 listed in Table S3 and cloned into *Bpi*I-linearized pICH41308[42] (Golden Gate entry
750 vector) by Gibson assembly (New England Biolabs). BAR and PAT coding sequences
751 were fused with *Agrobacterium tumefaciens* mannopine synthase promoter (from
752 pICH85281) and terminator (from pICH77901) into the empty binary vector pICH47732
753 by Golden Gate assembly[42]. pICH47732 constructs were transformed into *Agrobacterium*
754 *tumefaciens* GV3130 strain by electroporation and transformed into Arabidopsis Col-0 by
755 the floral dip method [43]. 90 mg of T1 seeds were sown on soil and transformants were
756 selected with Finale® (contains 11.33% glufosinate ammonium; Bayer CropScience)
757 diluted 1:500 in water. Photographs were taken 10 days after herbicide treatment (**Fig. 4**
758 and **Supplementary Fig. 12**). This experiment was repeated once with similar results. T2
759 seeds from 5 to 6 T1 plants were collected for each BAR mutants, sown on soil and
760 transgenic individuals were selected with Finale® (contains 11.33% glufosinate
761 ammonium; Bayer CropScience) diluted 1:500 in water (**Supplementary Fig. 13**). This

762 experiment was done once. Metabolites were extracted from dark-incubated leaves
763 collected from T2 phosphinothricin-resistant individuals (senescent leaves from 8-9
764 individuals were pooled for each T2 population) and then analyzed as described above
765 for the absolute quantification of acetyl-aminoadipate and acetyl-tryptophan in *Glycine*
766 *max* and *Brassica napus.*

767 To further compare the phosphinothricin tolerance in T2 lines transformed with
768 Y92F, N35T and wild-type BAR, seeds from 5-6 independent lines were germinated on
769 ½ MS medium containing 1% sucrose and 8 µg/mL glufosinate ammonium (45520-
770 Sigma-Aldrich). Seven-days old seedlings were then transformed on soil and further
771 grown for 10 days. Photographs were taken before treatment with four different
772 concentrations of Finale® (0, 0.2X, 1X and 5X; see **Supplementary Fig. 14** for further
773 details on the herbicide concentrations). Plants were further grown for 8 days,
774 photographs were taken and the average aerial mass of each T2 populations was
775 measured (average from 8-9 individuals). This experiment was done once.

776 Protein levels of the BAR mutants in T2 lines were measured as follow. For each
777 protein extraction, equal amounts of aerial tissues from 5-6 transgenic T2 populations
778 were pooled. Total proteins were isolated from frozen samples by homogenization in 5
779 volumes of ice-cold extraction buffer [50 mM Tris–HCl pH 8, 100 mM NaCl, 0.5% (v/v)
780 TritonX-100, 2mM β-mercaptoethanol] complemented with a protease inhibitor cocktail
781 (Complete; Roche Diagnostics). Samples were centrifuged at 12,000 g for 5 min and
782 protein concentration of the supernatant was determined using the Bradford Assay (Bio-
783 Rad). Proteins were subsequently precipitated with chloroform–methanol and 10 µg were
784 analyzed by SDS-PAGE and immunoblotting as described [44]. The following antibodies

were used for immunoblot analysis: a primary polyclonal antibody against BAR from *Streptomyces hygroscopicus* produced in rabbit (1:1000; P0374-Sigma-Aldrich) and a polyclonal horseradish peroxidase conjugated goat anti-rabbit IgG as the secondary antibody (1:50000; A0545-Sigma-Aldrich). Substrate detection was performed by chemiluminescence (ECL Western Blotting Substrate™ (Pierce)) and film exposure. This experiment was done once.

Data availability

The data that support the findings of this study are available from the corresponding authors upon reasonable request.

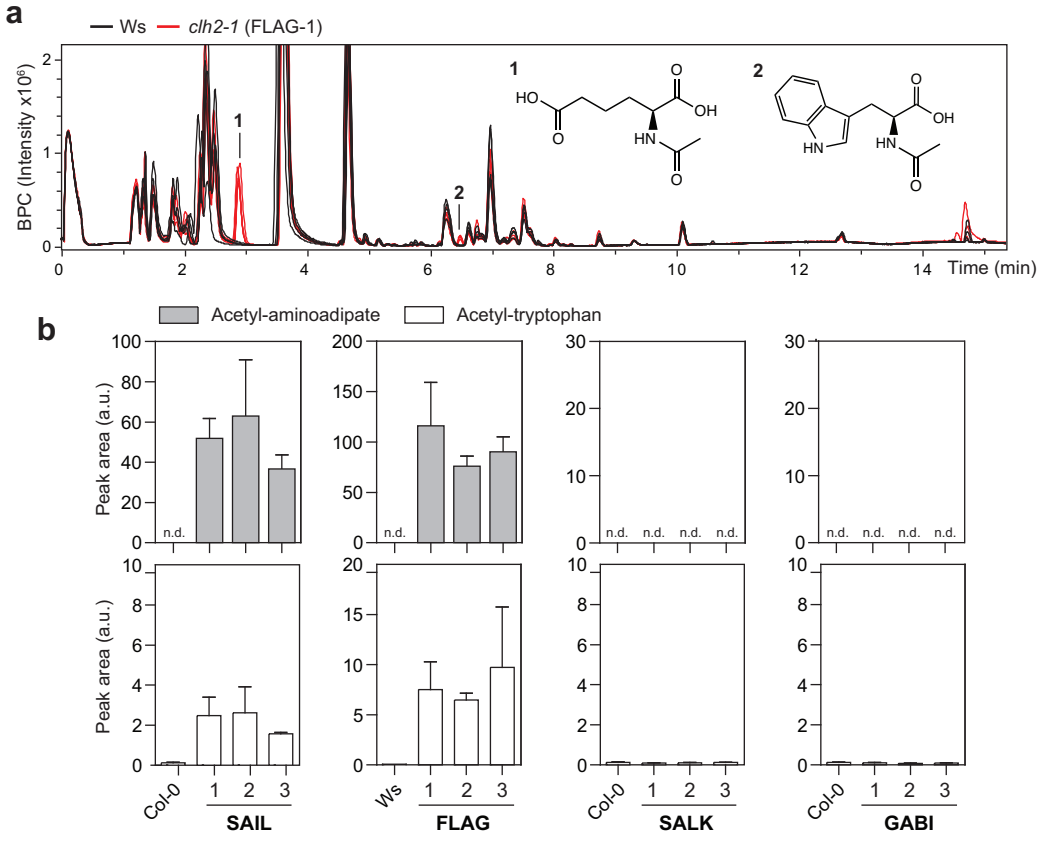

Figure 1 | Accumulation of acetyl-aminoadipate and acetyl-tryptophan in senescent leaves of Arabidopsis carrying the BAR transgene. a, Metabolite profiles of senescent leaves from Wassilewskija (Ws) and *clh2-1* (FLAG-1), displayed as base peak chromatograms (BPC), reveal the ectopic accumulation of acetyl-aminoadipate ('1') and acetyl-tryptophan ('2'). BPC traces of four biological replicates are displayed. **b**, Comparative levels of acetyl-aminoadipate and acetyl-tryptophan in Arabidopsis mutants from different insertional mutant collections that contain either BAR (SAIL and FLAG) or alternative selection marker genes (SALK (*NTPII*, kanamycin resistance) and GABI (*SULI*, sulfadiazine resistance)). Error bars, mean ± s.d. (n = 3 biological replicates). This experiment was repeated at least three times with similar results. See Supplementary Figure 2 for absolute quantification. a.u., arbitrary unit; FW, fresh weight; n.d., not detected

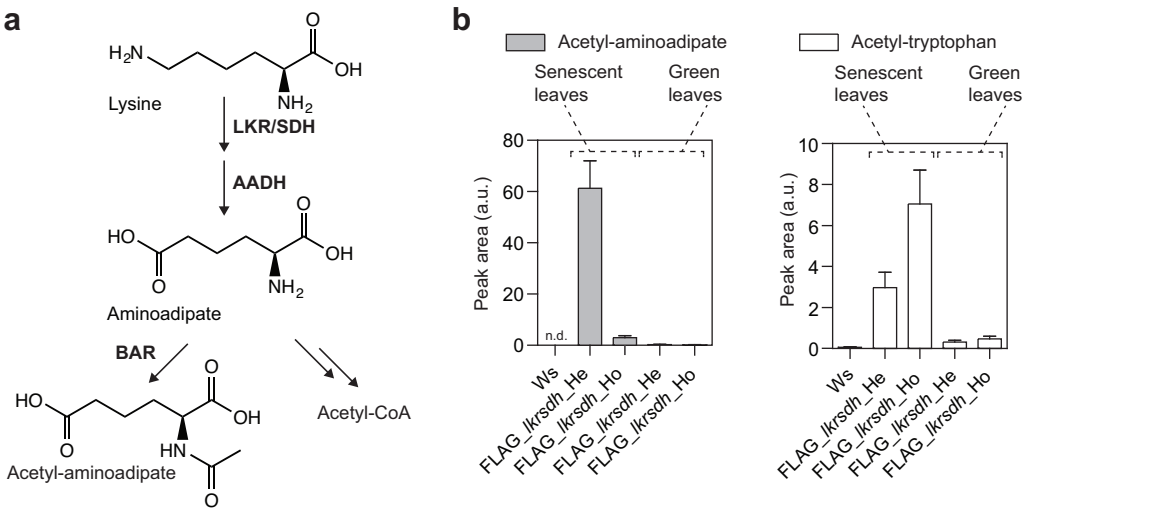

Figure 2 | BAR-dependent accumulation of acetyl-aminoadipate and acetyl-tryptophan is linked to nitrogen remobilization during senescence. a, Aminoadipate is derived from the lysine degradation pathway in plants, which can be metabolized by BAR as a nonspecific substrate. **b**, Comparative levels of acetyl-aminoadipate and acetyl-tryptophan in green and senescent leaves from the heterozygous (He) and homozygous (Ho) FLAG_*lkrsdh* mutant, harboring a BAR-containing T-DNA that abolishes the Arabidopsis *LKR/SDH* gene. Error bars, mean ± s.d. (n = 4 biological replicates). a.u., arbitrary unit; n.d., not detected; Ws, Wassilewskija wild-type plants.

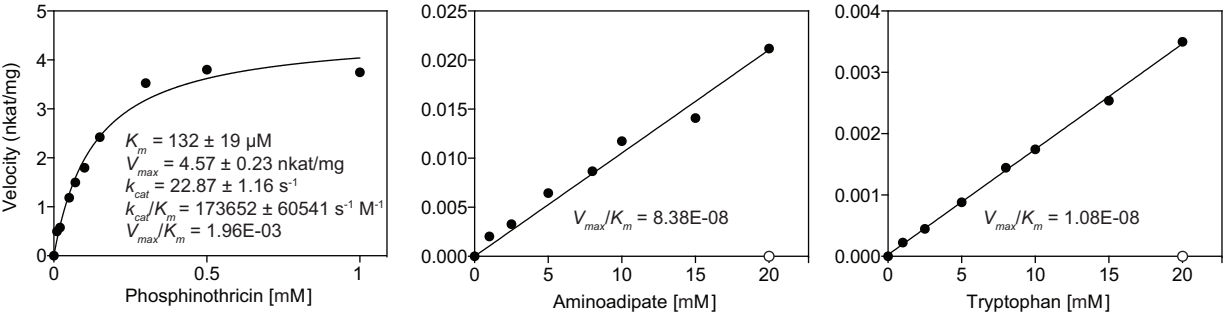

Figure 3 | *In vitro* enzyme kinetic assays of BAR against native and non-native substrates. An apparent K_M value of 132±19.2 µM was obtained for phosphinothricin, similar to previously published data[1, 3, 17]. V_{max}, k_{cat}, k_{cat}/K_m and V_{max}/K_m values for phosphinothricin are also indicated, as well V_{max}/K_m values for aminoadipate and tryptophan (estimated from Lineweaver-Burk plots). Aminoadipate and tryptophan are *in vitro* substrates of BAR but both substrates reached solubility limit before reaching saturation concentration for BAR. Negative controls (open circles) were performed in absence of BAR at the highest substrate concentration tested (20 mM).

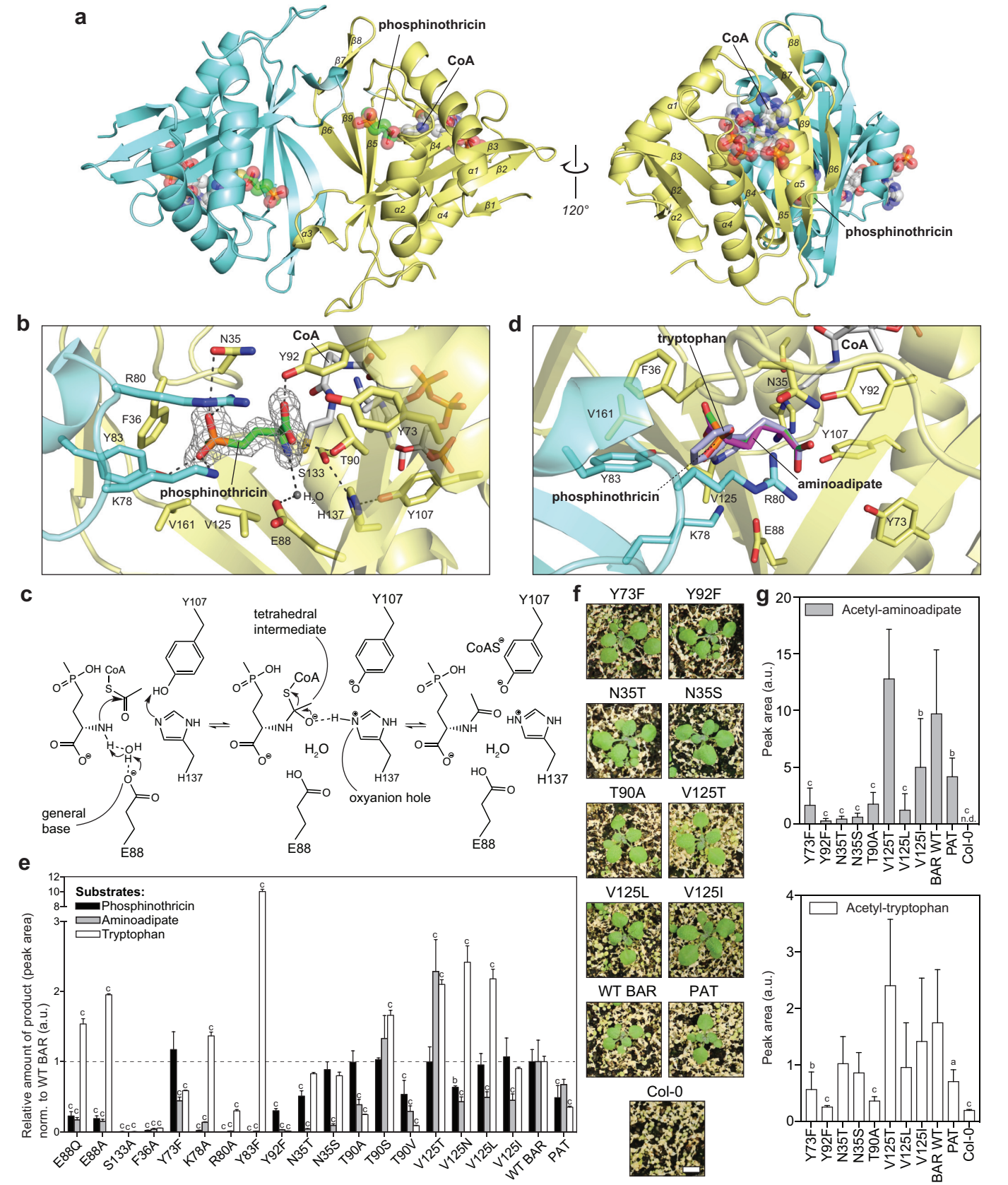

Figure 4 | Structural basis for amino acid N-acetylation catalyzed by BAR and structure-guided engineering of BAR with reduced nonspecific activities. a, Cartoon representation of BAR homodimer in complex with phosphinothricin and CoA. Two monomers of the dimer are colored in blue and yellow respectively. **b**, Close-up view of the BAR active site. The |2Fo-Fc| omit electron density map (contoured at 3.0 σ) is shown for phosphinothricin. **c**, Proposed catalytic mechanism of BAR. **d**, Docking of tryptophan and aminoadipate within the BAR active site reveals reduced favorable contacts compared to phosphinothricin. **e**, Enzyme activity assays using purified BAR mutant proteins against phosphinothricin (0.2 mM), aminoadipate (1 mM) and tryptophan (1 mM). Wild-type BAR (WT BAR) and PAT from *Streptomyces viridochromogenes* were also examined as controls. Assays were terminated during the initial linear rate of product formation. The relative amount of product formed by each BAR mutant was normalized to WT BAR for each substrate (value of 1). Error bars, mean ± s.d. (n = 3 technical replicates). **f**, Photographs of Arabidopsis T1 lines transformed with select BAR mutants 10 days after phosphinothricin treatment (see also Supplementary Fig. 12, 13 and 14). Scale bar = 0.3 cm. **g**, Comparative levels of acetyl-aminoadipate and acetyl-tryptophan in phosphinothricin-resistant T2 Arabidopsis plants transformed with selected BAR mutants. Error bars, mean ± s.d. (n = 5-6 biological replicates (Y73F (6), Y92F (6), N35T (5), N35S (5), T90A (6), V125T (5), V125L (6), V125I (6), WT BAR (5), PAT (5)). Significance levels were indicated based on one-way ANOVA with Dunnett's test for multiple comparisons to WT BAR. a, p-value<0.1; b, p-value<0.05; c, p-value<0.01; a.u., arbitrary unit.